Force and Stiffness Calculation and Optimization of Permanent Magnetic Thrust Bearing Used in Vessels

*Xingqian Zhao [a,b], Changgeng Shuai [a,b], Wei Xu [a,b], Demin Chen[c], Zechao Hu [a,b]

[a] Institute of Noise & Vibration, Naval University of Engineering, Wuhan, P.R. China, zhensheng711@foxmail.com (Wei Xu)
[b] National Key Laboratory of Ship Vibration and Noise, Wuhan, P.R. China
[c] Magna Drive Corporation, Beijing, P.R. China

***Abstract*—To isolate the vibration transmitted from the propeller to the vessel's hull, the main engine, the shaft together with the bearings are proposed to be installed on a large-scale isolation system. Permanent magnetic thrust bearing (PMTB) is applied to further reduce the vibration transmission. The Coulombian model is adopted to calculate the force and stiffness, which determine the application feasibility of the PMTB in vessels. Explicit computations are presented for stacked PMTB. The calculation result is compared with that obtained by finite element method (FEM) and experimentally tested. It is revealed that the Coulombian model is accurate enough and more economic than the FEM, which make it advantageous to the structure design and parameter optimization of PMTB. In the influence study by Coulombian model, it is found that the airgap width can exponentially change the maximum axial magnetic force and stiffness; the radial width is not a sensitive factor for both force and stiffness; the axial length should be 4/5 of the radial thickness to obtain the largest force and decent stiffness.**

I. INTRODUCTION

In marine propulsion system, the thrust bearing transforms the propeller's axial movement directly to the hull, which exciting the hull to vibrate and radiate sound. This will seriously reduce the quietness of the vessel and also cause negative influence on the marine organism [1, 2]. On another hand, traditional thrust bearing needs complicate lubrication system. To reduce the vibration and simplify the structure, the floating raft isolation system is adopted and the permanent magnetic thrust bearing (PMTB) is introduced to replace the traditional thrust bearing. As shown in Figure 1, the shaft system and all bearings are installed on a large raft which is connected with the vessel hull by vibration isolators.

Compared with traditional Michelle thrust bearings, the stiffness of PMTB decreases by one order of magnitude, from E^7 N/m to E^6 N/m. Lower stiffness means the shaft system will undergo larger displacement when transmitting the same thrust from the propeller. Furthermore, the stiffness of the thrust has great influence on the dynamic characteristics of the whole isolation system [3].

Permanent Magnetic Bearings (PMB), which are generally manufactured with axially or radially magnetized magnets, have the characteristics of no mechanical friction, low noise, low power-consumption and vibration reduction [4], so they are largely applied in the fields like space technology [5, 6], mechanical processing [7] and so on. Yonnet [8] is the pioneer in the study upon PMB, who calculated the magnetostatic energy created by a system of two magnets and obtained the expressions for forces by differentiate the energy expression with respect to the displacement. Beleggia [9-11] derived the general expression for the magnetostatic energy of two magnetic elements with arbitrary shape. Vokoun [12] continued the work of Beleggia and obtained analytical expressions for calculating the attraction force between two cylindrical permanent. The research achievement is utilized to continue research work in fields like magnetic guns [13], nonlinear energy sink [14], ultra-broad-band nonlinear acoustic metamaterials [15] and energy harvesting [16]. Another popular way to determine the magnetic force is based on Coulombian approach. It uses fictitious magnetic charge to model the magnetic field intensity. Rakotoarison [17] computed the demagnetization field in each point inside the permanent magnet and the magnetic fields outside it. Ravaud [18-20]determined the magnetic force exerted between rings axially or radially magnetized using Coulombian model.

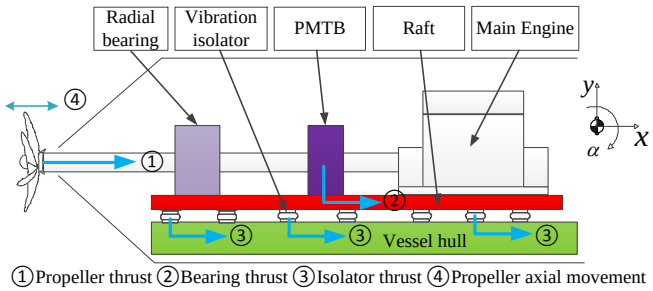

①Propeller thrust ②Bearing thrust ③Isolator thrust ④Propeller axial movement

Figure 1 Schematics of the isolation system for marine propulsion system

This paper firstly reviews the Coulombian approach for magnetostatic calculations and extends the results to obtain the magnetic force of large-scale stacked PMTB. Then, to verify the correctness of the calculating procedure, the numerical results from FEM and the tested results from a large-scale stacked PMTB are compared with that of Coulombian model and FEM method. Finally, the Coulombian model is used to analyze the influence of airgap width, radial thickness and layers on axial magnetic force and stiffness.

*Author: Xingqian Zhao (1989-), PhD candidate, Email: xqzhao0613@163.com
Corresponding auther: Wei Xu (1980-), Associate research fellow, E-mail: zhensheng711@foxmail.com

II. Force Calculation of PMTB Using Coulombian Model

A. Coulombian Model for Single Pair of Magnetic Ring

The derivative process is began with Maxwell's equations

$$\nabla\bullet\vec{E}=\rho/\varepsilon_0 \tag{1}$$

$$\nabla\bullet\vec{B}=0 \tag{2}$$

Eq. (1) is the Gauss's law and Eq. (2) is the Gauss's law for magnetism, both in differential form. The meaning the symbols are listed in the appendix in alphabetical order.

Ferromagnetic materials have the property of

$$\vec{B}=\mu_0\vec{H}+\vec{J} \tag{3}$$

where J is the magnetic polarization, which represents the vector sum of magnetic dipole moment in unit volume. By combining Eq. (2) and Eq. (3)

$$\nabla\bullet\vec{H}=-\nabla\bullet\vec{J}/\varepsilon_0 \tag{4}$$

From Eq. (2), it is known that there is no monopole magnetic charge which can create magnetic field individually, but corresponding to electrical charge, we imagine fictitious magnetic charge σ distributing on the surface of and inside permanent magnets, which are indicated by σ_v and σ_s respectively. By comparing Eq. (4) with Eq. (1), the fictitious magnetic charge density is

$$\sigma=-\nabla\bullet\vec{J} \tag{5}$$

If the magnetic rings of the PMTB are radially magnetized and the magnetic polarization J is uniform, then the expression of J in cylindrical coordinate system is

$$\vec{J}=(J,0,0) \tag{6}$$

then the expression of σ_v is

$$\sigma_v=-\nabla\bullet\vec{J}=-\frac{1}{r}\frac{\partial(rJ_r)}{\partial r}-\frac{1}{r}\frac{\partial(J_\theta)}{\partial\theta}-\frac{\partial(J_z)}{\partial z}=-\frac{J}{r} \tag{7}$$

As discussed above, there is no monopole magnetic charge for an entire magnetic ring, so

$$\iint_s\sigma_s ds+\iiint_v\sigma_v dv=0 \tag{8}$$

From Gauss's theorem

$$\iiint_\Omega\nabla\bullet\vec{F}dV=\iint_{\partial\Omega}\vec{F}\bullet\vec{n}ds \tag{9}$$

Identified from Eq. (7), (8), (9), it is obtained that

$$\sigma_s=\vec{J}\bullet\vec{n} \tag{10}$$

For a pair of magnetic rings, as shown in Figure 1, the inner ring is attached to the rotator and the outer ring to the stator. The axial force is the sum of magnetic force between surface and surface, volume and surface, volume and volume, which can be written as

$$F_z=F_z(\mathrm{s-s})+F_z(v-\mathrm{s})+F_z(v-v) \tag{11}$$

where

$$F_z(\mathrm{s-s})=\sum_{i=1,2}\sum_{j=3,4}\int_{\theta_1=0}^{2\pi}\int_{z_1=0}^{h}\int_{\theta_2=0}^{2\pi}\int_{z_2=z_a}^{z_b}(-1)^{i+j}A(r_i,r_j)\times dz_1d\theta_1dz_2d\theta_2 \tag{12}$$

$$F_z(v-\mathrm{s})=\sum_{j=3,4}\int_{r_{out}=r_2}^{r_1}\int_{\theta_1=0}^{2\pi}\int_{z_1=0}^{h}\int_{\theta_2=0}^{2\pi}\int_{z_2=z_a}^{z_b}(-1)^{j}\times B(r_j,r_{out})\,dr_{out}dz_1d\theta_1dz_2d\theta_2+\sum_{i=1,2}\int_{r_{in}=r_4}^{r_3}\int_{\theta_1=0}^{2\pi}\int_{z_1=0}^{h}\int_{\theta_2=0}^{2\pi}\int_{z_2=z_a}^{z_b}(-1)^{i}\times B(r_i,r_{in})\,dr_{in}dz_1d\theta_1dz_2d\theta_2 \tag{13}$$

$$F_z(v-v)=\sum_{i=1,2}\int_{r_{out}=r_2}^{r_1}\int_{r_{in}=r_4}^{r_3}\int_{\theta_1=0}^{2\pi}\int_{z_1=0}^{h}\int_{\theta_2=0}^{2\pi}\int_{z_2=z_a}^{z_b}C(r_i,r_{in})\times dr_{in}dz_1d\theta_1dz_2d\theta_2 \tag{14}$$

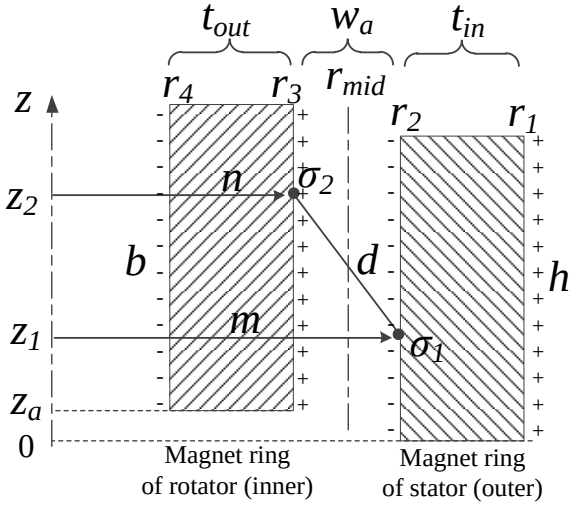

Figure 2 Sectional view of a pair of magnetic ring. The outer ring is attached to the stator and the inner ring is attached to the rotator. The inner ring can move axially. Both rings are radially magnetized.

We first consider the situation when two fictitious magnetic charges located on the surfaces, as shown in Figure 1. Compared with Coulomb's law, the magnetic force is

$$A(m,n)=\frac{\sigma_1\sigma_2}{4\pi\mu_0 d^2}\bullet\frac{z_2-z_1}{d}\bullet mn \tag{15}$$

where

$$d=\sqrt{(m-n)^2+(z_2-z_1)^2} \tag{16}$$

considering Eq. (7) and (10), it is obtained

$$B(m,n)=\frac{A(m,n)}{n},\quad C(m,n)=\frac{A(m,n)}{mn} \tag{17}$$

substitute Eq. (12)-(17) in to Eq. (11), we can obtain the entire axial force generated by a pair of magnetic rings. It is obvious that the expressions of Eq. (12), (13), (14) which include quadruple, quintuple or sextuple integrals, are very complicated and it is impossible to obtain the analytical results [19]. If we totally adopt numerical method, the computational cost will be too high, so the efficient and feasible way is to finish part of the multiple integrals analytically and utilize numerical integral to calculate the rest part.

After calculation, we found that the results of Eq. (13) and (14) are much smaller than that of Eq. (12). The ratios of peak values are less than 1%, so to further reduce the computational cost, we only calculate the magnetic force between surface and surface and ignore the other two parts.

B. *Force Calculation for Stacked PMTB*

Next step, we consider the stacked structure, as shown in Figure 3. The magnetic rings of the stator (outer) are fixed on the bearing block and the magnetic rings of the rotator (inner) are connected with the shaft which can move axially. All the magnetic rings are radially and uniformly magnetized with the same orientation.

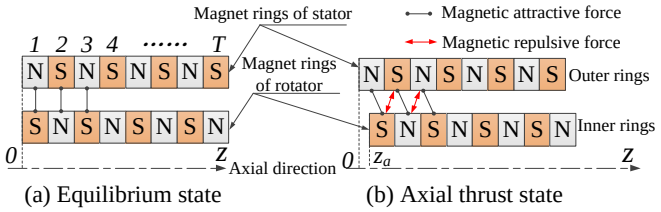

(a) Equilibrium state (b) Axial thrust state

Figure 3 Schematic diagram of the permanent magnetic thrust bearing

In equilibrium (Figure 3 (a)), the magnetic rings do not provide axial force. When the propeller thrust drives the rotator magnetic rings to move in the axial direction, as shown in Figure 3 (b), the induced magnetic attractive and repulsive forces make it produce axial thrust.

In the stacked structure, every two magnetic rings of inner and outer ones generate magnetic forces. If the PETB consists of T pairs of magnetic rings, then all the magnetic forces can be written in a matrix form as follows

$$\mathbf{F} = \left[F_{pq} \right]_{T\times T} \tag{18}$$

where

$$F_{pq} = (-1)^{p+q} \sum_{i=1,2} \sum_{j=3,4} \int_{\theta_1=0}^{2\pi} \int_{z_1=0}^{h} \int_{\theta_2=0}^{2\pi} \int_{z_2=z_{pq}}^{z_{pq}+b} (-1)^{i+j} \times A(r_i, r_j) dz_1 d\theta_1 dz_2 d\theta_2 \tag{19}$$

where

$$z_{pq} = z_a - h(p-1) + b(q-1) \tag{20}$$

The total axial force exerted by the PMTB is the sum of **F** elements

$$F_{entire} = \sum_{p=1}^{T} \sum_{q=1}^{T} F_{pq} \tag{21}$$

C. *Stiffness Calculation for Stacked PMTB*

The stiffness of PMTB is very important for the dynamic characteristics of marine propulsion system. The value of stiffness can be obtained from computing the gradient of the force to displacement. When concentrating on the axial stiffness, it becomes calculating the derivative of axial force F_{entire} to axial displacement z_a

$$K_z = -\partial F_{entire} / \partial z_a \tag{22}$$

III. Force Calculation of PMTB Using FEM

The FEM simulation is implemented by Comsol Multiphysics through the physic field of "Magnetic field, No current". The software takes advantage of rotational symmetry of the PMTB and a 2D model is adopted to reduce the computational cost. The principle of the magnetic force calculation is to obtain the magnetic induction distribution through Maxwell stress tensor method [13, 21]. Maxwell stress tensor T_{ij} is expressed as

$$T_{ij} = \frac{1}{\mu_0} B_i B_j - \frac{1}{2\mu_0} B_{ij}^2 \delta_{ij} \tag{23}$$

Where, δ_{ij} is the Kronecker delta function. Then the force is computed by

$$\mathbf{F} = \int_{\partial\Omega} 2\pi r \vec{\mathbf{n}} T dS \tag{24}$$

where $\vec{\mathbf{n}}$ is the surface normal vector and the integration is conducted over the surface of region Ω. In Comsol, the stiffness calculation is also based on computing the gradient of magnetic force with respect to displacement vector. The physical field of "sensitivity" is applied to complete the stiffness calculation. It should be mentioned that we only calculate the axial magnetic stiffness, so the 2D model is sufficient. If calculating the magnetic stiffness in radial direction or coupled stiffness coefficients, a complete 3D model is required.

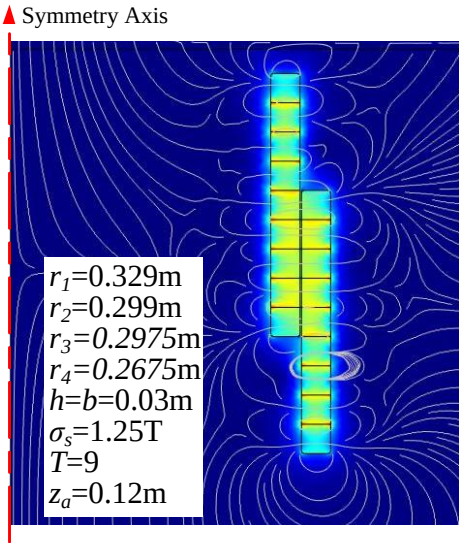

Figure 4 Magnetic force calculation of stacked PMTB using FEM in Comsol Multiphysics

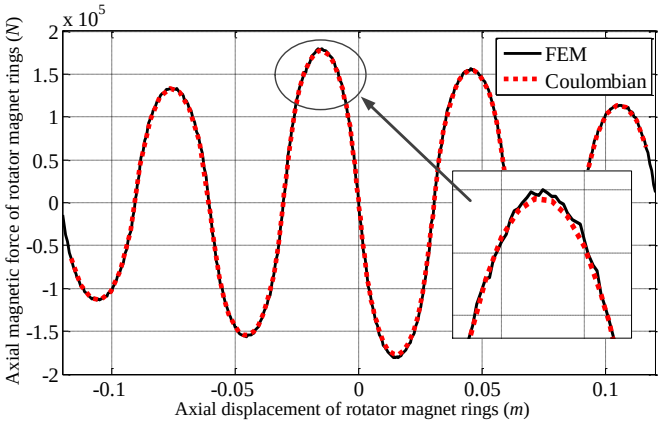

Figure 5 Diagram of the magnetic force versus axial displacement calculated by FEM and Coulombia model.

The force calculation results by two methods are illustrated in Figure 5. It shows that both methods give almost identical force curves. Only at the peaks or valleys, the values of Coulombian model are a little smaller than that of FEM, but it is obvious that the FEM curve is not as smooth as the one gener-

ated by Coulombian model. In the FEM calculation, the 2D model is meshed into 6850 elements. If finer mesh is used, the FEM curve can be smoother, but more elements means more time-cost.

The stiffness calculation results comparation is shown in Figure 6. It is apparent that the unevenness of FEM force curve leads to the stiffness curve much unsmoother. This also cause the FEM fails to predict the magnet stiffness at the valleys, namely when the axial displacement equals an integral multiple of the axial length of magnetic ring h (b=h). But apart from the parts around the valleys, the two curves have similar values for most axial displacement.

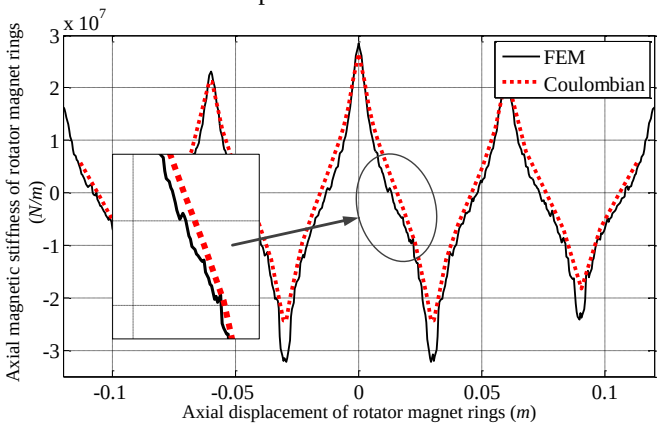

Figure 6 Diagram of the magnetic stiffness versus axial displacement calculated by FEM and Coulombia model.

Moreover, even though using a 2D model, the computing process of FEM still costs around 2 hours, while it costs only 6 minutes by Coulombian model by the same computer. We can conclude that the Coulombian model yields physically reasonable force calculation results in much smaller time-cost.

IV. Experimental Results

NdFeB is adopted as the permanent magnetic material to manufacture an experimental prototype of the PMTB. Figure 7 illustrates the experimental setup for the axial magnetic force measurement. The outer magnetic rings are fixed to the stator (bearing block) of the PMTB and the inner rings are attached to the rotator (shaft) of the PMTB. One end of the PMTB rotator is attached with the motor through a flexible coupling. The other end is connected to an axial loading, which is a hydraulic pump. At the beginning of the experiment, the motor drove the shaft to rotate and the hydraulic pressure was set to zero. During the measurement, we recorded the exerted force every 1mm of the rotator axial displacement. The measurement was conducted three times and the relationship between the applied load and the axial displacement was obtained by averaging the data.

The tested axial magnetic force compared with the negative magnetic forces calculated by Coulombian model and FEM is shown in Figure 8, in which only the comparation above the x axis is illustrated because of symmetry. It is shown that the values obtained by both the Coulombian model and the FEM are reasonably close to the corresponding measurements. Deviations are expected and acceptable because the calculations by Coulombian approach and FEM are based on the uniform magnetization approximation. It proves that both the Coulombian model and FEM simulation have sufficient accuracy for the axial force prediction of the PMTB.

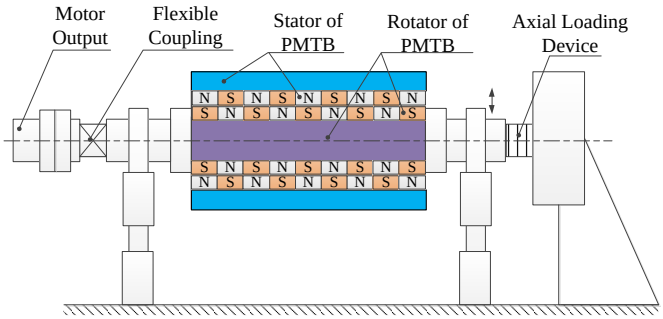

Figure 7 Schematic diagram of the experimental apparatus for the measurement of PMTB axial magnetic force

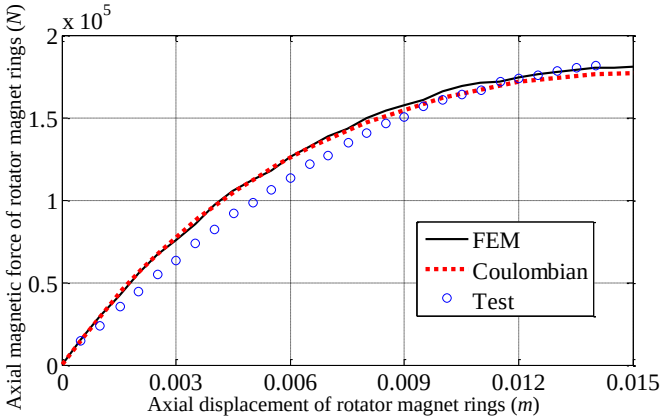

Figure 8 Diagram of the magnetic force versus axial displacement calculated by FEM, Coulombia model and tested results

Central difference method is applied to deal with the tested data and obtain the magnetic stiffness. The results Comparation is shown in Figure 9. It is revealed that for most values, the result of FEM is smaller than that of tested and the values computed by Comlombian is close to the ones by tested, so the Coulombian model has better prediction upon magnetic stiffness than the FEM with less time-cost.

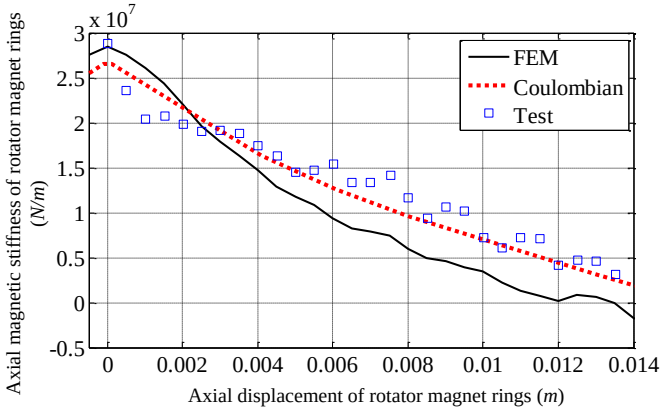

Figure 9 Diagram of the magnetic stiffness versus axial displacement calculated by FEM, Coulombia model and tested results

After comparing the results of FEM, Coulombian model and tested, we conclude that both calculation methods can

well determine the magnetic force and the Coulombian model can get smoother curve than FEM. Upon stiffness determination, Coulombian model is preciser than FEM. It also reveals that in Coulombian model only considering the reaction between faces is accurate enough in the PMTB design.

V. Parameter Pptimization of PMTB

In this section, the Coulombian model is used to study the influence of PMTB structural parameters on the magnetic force and stiffness, including the airgap width, the radial thickness difference and the axial length of magnetic ring.

A. *influence of airgap width*

When calculating the magnetic force and stiffness for different airgap widths w_a between the outer and inner rings, the influence of other structural parameters should be minimized. Eq. (12) reveals that the surface area of the magnetic rings is a determinative factor in Coulombian model, so to reduce its influence we keep the middle position of the airgap r_d constant, in which way the outer and inner rings variation of surface area can offset each other.

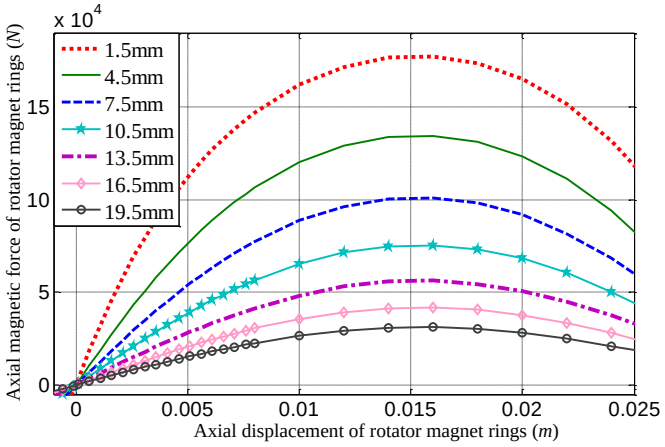

Figure 10 Diagram of the magnetic force versus axial displacement exerted between 9-layer stacked magnetic rings for different air gaps: r_{mid} =0.29825m, t_{out}= t_{in}=0.03m, σ_s=1.25T, h=b =0.03m.

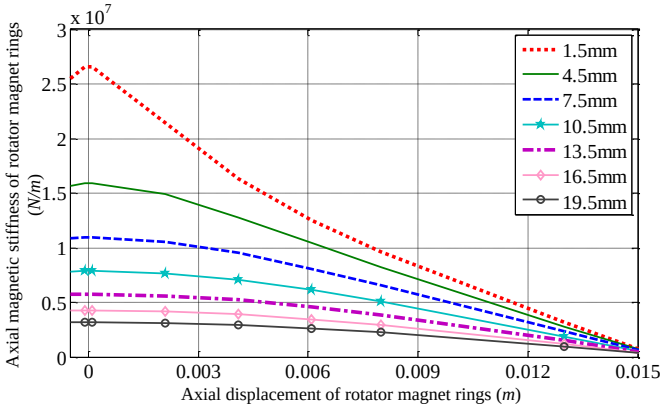

Figure 11 Diagram of the magnetic stiffness versus axial displacement exerted between 9-layer stacked magnetic rings for different air gaps: r_{mid} =0.29825m, t_{out}= t_{in}=0.03m, σ_s=1.25T, h=b =0.03m.

Figure 10 and Figure 11 illustrate the axial magnetic force and stiffness versus displacement when w_a varies from 1.5mm to 19.5mm, which means the ratio between w_a and radial thickness of magnetic rings t_{out} (t_{in}) varies from 5% to 65%. It is obvious that the increment of w_a can reduce the axial force and stiffness greatly. The maximum forces and stiffnesses are extracted and ploted in Figure 12 versus w_a. Through curve fitting, an function of

$$f(x) = 2.058e^{5} \times e^{-0.09565x} \quad (25)$$

is obtained whose curve (the blue line in Figure 12) can perfectly cover all maximum force points. This gives the conclusion that the axial magnetic force decreases exponentially with the increment of airgap width. We can see that the stiffness has the similar tendency with the force.

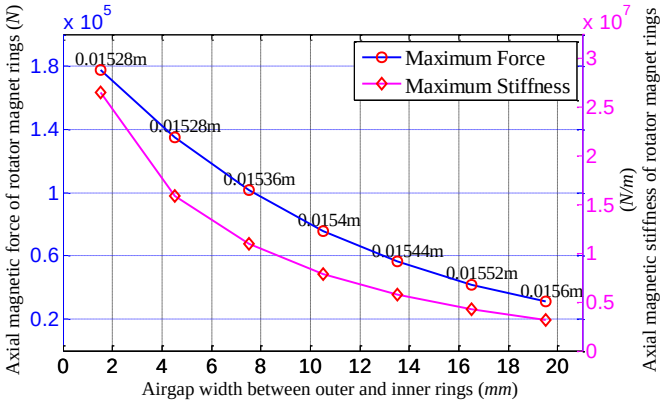

Figure 12 Diagram of the maximum magnetic force and stiffness versus airgap width exerted between 9-layer stacked magnetic rings: r_{mid} =0.29825m, t_{out}=t_{in}=0.03m, σ_s=1.25T, h=b=0.03m. The axial displacement where the maximum forces occur are labeled near the corresponding point.

In Figure 12, the axial position where the maximum forces occur are labeled near the corresponding point which reveals that increasing airgap width can slightly alter the maximum force towards larger displacement. It is also found that increasing the number of layers T can minimize the position alternation. Generally, a PMTB is comprised of more than ten layers of magnetic rings, so we believe that this influence can be neglect in the PMTB design.

B. *influence of radial thickness*

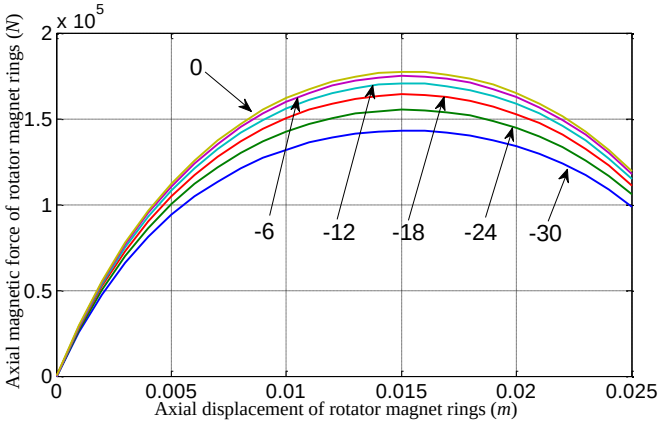

Figure 13 Diagram of the magnetic force versus axial displacement exerted between 9-layer stacked magnetic rings for different r_d (the unit is mm): r_1=0.329m, r_4=0.2675m, w_a =0.0015m, σ_s=1.25T, h=b=0.03m.

During the calculation, the total volume of all magnetic rings is kept constant, namely $t_{in}+t_{out}$=0.06m and w_a =1.5mm. In the study of this section, the value of radial thickness difference r_d =t_{in}-t_{out} changes from -30mm to 30mm. Figure 13 and Figure 14 illustrate the axial magnetic force and stiffness versus displacement for r_d varies from -30mm to 0mm and from 0mm to 30mm, respectively. Actually, for inner or outer magnetic ring, r_d =30mm or -30mm means the radial thickness has increased or decreased 50%, which is a huge variation, but the magnetic force and stiffness don't have dramatic change, so the radial thickness change is not an sensitive factor for magnetic force and stiffness.

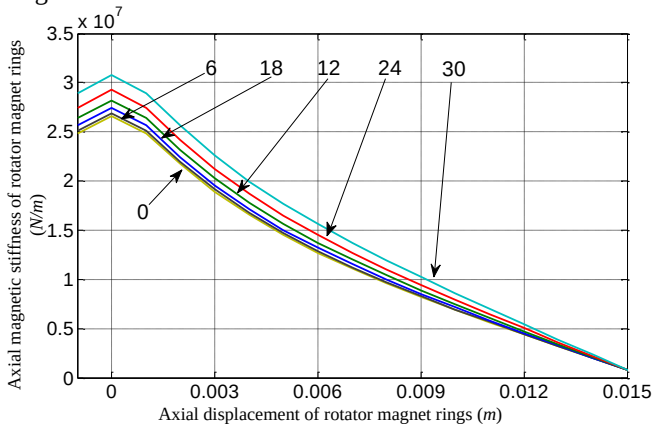

Figure 14 Diagram of the magnetic stiffness versus axial displacement exerted between 9-layer stacked magnetic rings for different r_d (the unit is mm): r_1=0.329m, r_4=0.2675m, w_a =0.0015m, σ_s=1.25T, h=b =0.03m.

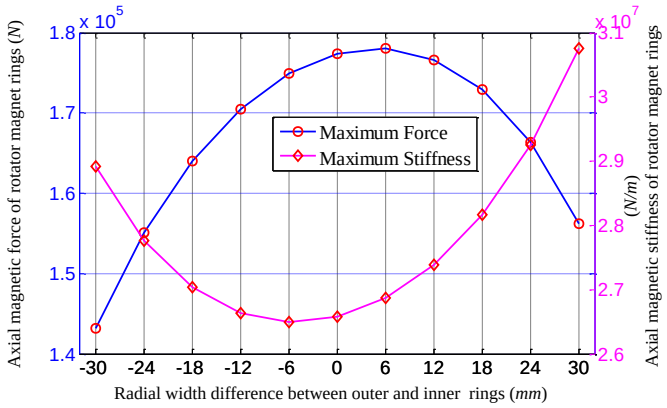

Figure 15 Diagram of the maximum magnetic force and stiffness versus the thickness difference r_d: r_1=0.329m, r_4=0.2675m, w_a= 0.0015m, σ_s=1.25T, h=b =0.03m.

From Figure 15, we find that the largest magnetic force does not appear at r_d=0, namely t_{in}=t_{out}, but occurs where the inner ring thickness a bit larger than the outer one. The tendency of the stiffness is unexpected. The maximum stiffness versus r_d appears an inverse tendency compared with the one of force.

C. influence of axial length of single magnetic ring

In the study of this part, the total volume of all magnetic rings is still kept constant. At the same time, we kept h=b, t_{in}=t_{out} =0.03m and the total axial length of magnetic rings L=0.24m). In the calculation, the rings are divided into different layers to calculate the axial magnetic force and stiffness. *ss*, the ratio between axial length and radial width of single magnetic layer, is used to describe the change of axial length of single layer. Figure 16 and Figure 17 demonstrate the force and stiffness versus axial displacement exerted between magnetic rings of different *ss*. From Figure 12 it is concluded that the maximum magnetic force appear at almost half of h (b), so the variation of axial length can dramatically change the position where the maximum occur, which will further determine the range of axial displacement of the rotator. From Figure 17, it is revealed that increasing T, decreasing h and b can improve the stiffness. For a PMTB, the available axial displacement is strictly limited, so we can meet the demand through increasing layers and decreasing axial length of magnetic rings.

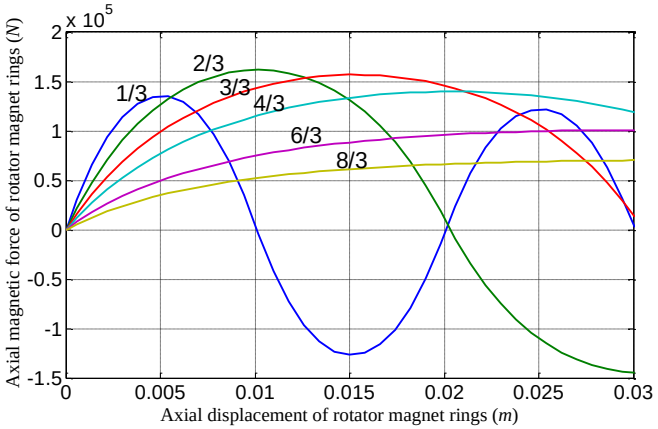

Figure 16 Diagram of the magnetic force versus axial displacement exerted between magnetic rings of different layers: r_1=0.329m, r_2=0.299m, r_3=0.2975m, r_4=0.2675m, σ_s=1.25T, t_{in} = t_{out} =0.03m, L=0.24m T=[24, 12, 8, 6, 4, 3]. *ss* are labeled near the corresponding curves.

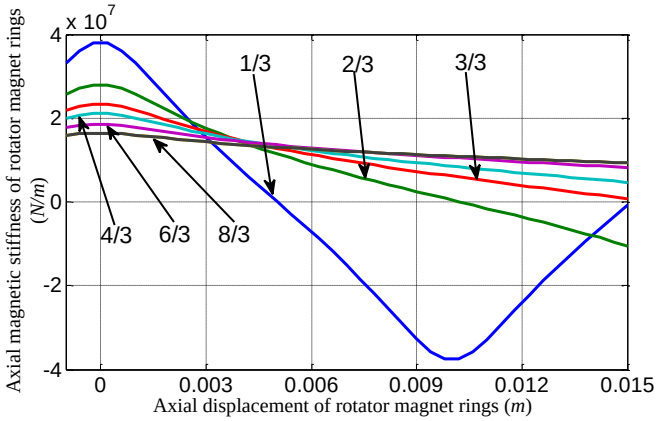

Figure 17 Diagram of the magnetic stiffness versus axial displacement exerted between magnetic rings of different layers: r_1=0.329m, r_2=0.299m, r_3=0.2975m, r_4=0.2675m, σ_s=1.25T, t_{in} = t_{out} =0.03m, L=0.24m, T=[24, 12, 8, 6, 4, 3]. *ss* are labeled near the corresponding curves.

Maximum magnetic force and stiffness versus *ss* are shown in Figure 18. It is found that the maximum magnetic force occur at point where the h (b) equals around 4/5* t_{out} (t_{in}). Besides, the maximum stiffness monotonically decreases with increasing *ss*. When *ss* less than 1, the stiffness will change

dramatically, so in this range, *ss* is an sensitive factor for magnetic stiffness.

D. Obtaining the optimal structural parameters

From the above analysis, it is concluded that the airgap width w_a can reduce the magnetic force and stiffness exponentially, so smaller w_a is favorable for PMTB design. The specific value of w_a should be determined based on the dimension of magnetic rings. For example, the w_a should be among 1mm to 3mm for rings with 30mm square section.

The radial thickness (t_{out}, t_{in}) is not a sensitive factor for both force and stiffness, so PMTB can be designed as t_{out}=t_{in}.

The layers or the axial length is a sensitive factor for both the force and stiffness. Especially, it determines the axial moving range of rotator when bearing thrust from the propeller. To maximize the axial magnetic force and meanwhile get large enough stiffness, the ratio between h (b) and t_{out} (t_{in}) should be around 4/5.

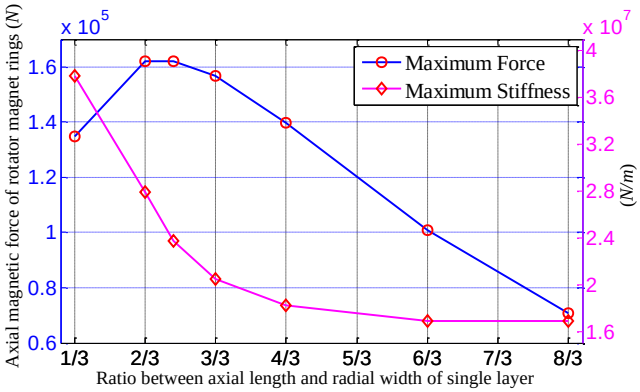

Figure 18 Diagram of the maximum magnetic force and stiffness versus the ratios between axial length and radial width of single magnetic layer *ss*: r_1=0.329m, r_2=0.299m, r_3=0.2975m, r_4=0.2675m, σ_s=1.25T, t_{in} = t_{out} =0.03m, L=0.24m, T=[24, 12, 8, 6, 4, 3].

VI. Discussions

This paper provides a feasible method, the Coulombian approach, for the design of PMTB. To verify the accuracy of the Coulombian model, the calculated results are first compared with that from FEM. It is revealed that both methods present almost identical force curves. However, the unevenness of FEM force curve not only leads to the stiffness curve much unsmoother, but also fails to predict the magnet stiffness at the values around curve valleys. A large-scale stacked PMTB was manufactured and the tested results from the experiment further verify the correctness of Coulombian model. So it can be concluded that the Coulombian model has precise enough prediction of magnetic force and stiffness in much smaller time-cost than FEM, which makes it advantageous to the structure design and parameter optimization of PMTB.

In the influence study by Coulombian model, it is found that the airgap width and axial length of magnetic rings are pretty sensitive parameters for the force and stiffness. The former one has an exponential relationship with the force and stiffness and the latter one can change the range of available axial displacement for a PMTB. However, the impact of radial thickness is not so obvious and can choose the same thickness of outer and inner rings. All these conclusions can be very important in the design of PMTB.

Acknowledgments

This work was financially supported by Natural Science Fund 51705529 and National Science Key Lab Fund 61422040601162204004.

Appendix

B: magnetic induction intensity
E: electric field
F_z: axial magnetic force
F_z(*s-s*): axial magnetic force between surface and surface
F_z(*v-s*): axial magnetic force between volume and surface
F_z(*v-v*): axial magnetic force between volume and volume
F: Force matrix whose element is the magnetic force between every pair of magnetic rings
F_{pq}: the magnetic force between No. p outer ring and No. q inner ring
F_{entire}: the entire force of the stacked PMTB
H: magnetic field
h, b: axial length of the outer (stator) or inner (rotator) magnetic rings
J: magnetic polarization
K_z: axial stiffness
L: the total axial length of all stacked magnetic rings.
m, n: radial component of a fictitious magnetic charge located in the outer or inner magnetic ring
$\vec{\mathbf{n}}$: unit normal vector of surface
p, q: the sequence number of the outer or the inner ring
r_1, r_2: outer and inner radii of the outer magnetic ring (stator)
r_3, r_4: outer and inner radii of the inner magnetic ring (rotator)
r_d: the radial thickness difference between inner and outer rings, $r_d = t_{in}- t_{out}$
r_{mid}: radius of the airgap middle position, namely the mean value of r_2 and r_3
ss: the ratio between axial length and radial width of single magnetic layer, namely $ss=h/(r_1-r_2)=b/(r_3-r_4)$
T: the number of the pairs of magnetic rings in stacked PMTB
t_{out}: the thickness of outer ring, $t_{out}= r_1-r_2$
t_{in}: the thickness of inner ring, $t_{in}= r_3-r_4$
w_a: the width of the airgap between the outer and inner rings
z_1, z_2: axial component of a fictitious magnetic charge located in the outer or inner magnetic ring
z_a, z_b: axial position of the lower and upper surface of the No. 1 inner magnetic ring (rotator)
z_{pq}: the relative axial position of No. p outer ring and No. q inner ring
ρ: electrical charge density
σ: factitious magnetic charge density
σ_v: factitious magnetic volume charge density
σ_s: factitious magnetic surface charge density
μ_0: vacuum permittivity
ε_0: vacuum permeability
Ω: bounded closed region
$\partial\Omega$: the boundary of Ω
θ_1, θ_2: azimuthal component of a fictitious magnetic charge located in the outer or inner magnetic rings

References

[1] J. Pan, N. Farag, T. Lin, and R. Juniper, "Propeller induced structural vibration through the thrust beraing," *Acoustics 2002-Innovation in Acoustics and Vibration Annual Conference of the Australian Acoustical Society*, pp. 2002.

[2] Y. Qiang,W. Lei and L. Wei, "Transmission characteristics of propeller

excitation for naval marine propulsion shafting," *Chinese Journal of Ship Research*, vol. 10, no. 6, pp. 81-86, 94, 2015.
[3] Y. Jiayou, "Research on characteristics of fluid film stiffness of water-lubricated bearings and the influence on shafting vibration", *Harbin Engineering University*, 2013.
[4] T. Lulin, L. Yan, W. Shan-shi, and Y. Jing, "Research on magnetism engineering analytical calculation method for bi-barrel-shaped radial permanent magnetic bearings," *Proseedings of the CSEE*, vol. 27, no. 6, pp. 2007.
[5] T. Ohji, S. C. Mukhopadhyay, M. Iwahara, and S. Yamada, "Performance of repulsive type magnetic bearing system under non-uniform magnetization of permanent magnet," *Ieee T. Magn.*, vol. 36, no. 5, pp. 3696-3698, 2000.
[6] B. Paden,N. Groom and J. Antaki, "Design formulas for permanent magnet bearing," *J. Mech. Design*, vol. 125734-738, 2003.
[7] T. Ohji, S. Ichiyama, K. Amei, M. Sakui, and S. Yamada, "A new conveyor system based on a passive magnetic levitation unit having repulsive-type magnetic bearings," *ournal of magnetism and magnetic materials*, vol. 2721731-1733, 2004.
[8] J. YONNET, "Permanent magnetic bearings and couplings," *TRANSACTIONS ON MAGNETICS*, vol. 17, no. 1, pp. 1169-1173, 1981.
[9] M. Beleggia, S. Tandon, Y. Zhu, and M. De Graef, "On the magnetostatic interactions between nanoparticles of-85," *J. Magn. Magn. Mater.*, vol. 278270-284, 2004.
[10] M. Beleggia and M. De Graef, "General magnetostatic shape – shape interactions," *J. Magn. Magn. Mater.*, vol. 285L1-L10, 2005.
[11] M. Beleggia,D. Vokoun and M. De Graef, "Demagnetization factors for cylindrical shells and related shapes," *J. Magn. Magn. Mater.*, vol. 3211306-1315, 2009.
[12] D. Vokoun, M. Beleggia, L. Heller, and P. Sittner, "Magnetostatic interactions and forces between cylindrical permanent magnets," *J. Magn. Magn. Mater.*, vol. 3213758-3763, 2009.
[13] D. Vokoun,M. Beleggia and L. Heller, "Magnetic guns with cylindrical permanent magnets," *J. Magn. Magn. Mater.*, vol. 3241715-1719, 2012.
[14] X. Fang, J. Wen, J. Yin, and D. Yu, "Highly efficient continuous bistable nonlinear energy sink highly efficient continuous bistable nonlinear energy sink," *Nolinear Dynamics*, vol. 87, no. 4, pp. 1-19, 2016.
[15] X. Fang, J. Wen, B. Bonello, J. Yin, and D. Yu, "Ultra-low and ultra-broad-band nonlinear acoustic metamaterials," *Nature Communications*, vol. 8, no. 1, pp. 1-11, 2017.
[16] P. V. Avvari, L. Tang, Y. Yang, and C. K. Soh, "Enhancement of piezoelectric energy harvesting with multi-stable nonlinear vibrations," *processings of SPIE*, vol. 868886881H-86882H, 2013.
[17] H. L. Rakotoarison,J. P. Yonnet and B. Delinchant, "Using coulombian approach for modeling scalar potential and magnetic field of a permanent magnet with radial polarization," *Ieee T. Magn.*, vol. 43, no. 4, pp. 1261-1264, 2007.
[18] R. Ravaud,G. Lemarquand and V. Lemarquand, "Force and stiness of passive magnetic bearings using permanent magnets. Part 1: axial magnetization," *Ieee T. Magn.*, vol. 45, no. 7, pp. 2996, 2009.
[19] R. Ravaud,G. Lemarquand and V. Lemarquand, "Force and stiffness of passive magnetic bearings using permanent magnets. Part 2: radial magnetization," *Ieee T. Magn.*, vol. 45, no. 9, pp. 3334-3342, 2009.
[20] R. Ravaud and G. Lemarquand, "Halbach structures for permanent magnets bearings," *Progress In Electromagnetics Research M*, vol. 14263-277, 2010.
[21] E. P. FURLANI, *Permanent magnet and electromechanical devices*, Acamedic Press, 2001.